

# The Hanle effect and level crossing spectroscopy in Rb vapour under strong laser excitation

Janis Alnis<sup>1</sup>, Kaspars Blushs<sup>1</sup>, Marcis Auzinsh<sup>1</sup>, Sharon Kennedy<sup>2</sup>,  
Neil Shafer-Ray<sup>2</sup> and E R I Abraham<sup>2</sup>

<sup>1</sup> Department of Physics, University of Latvia, 19 Rainis Boulevard, Riga, LV-1586, Latvia

<sup>2</sup> Department of Physics and Astronomy, The University of Oklahoma, Norman, OK 73019, USA

Received 12 December 2002, in final form 30 January 2003

Published 26 February 2003

Online at [stacks.iop.org/JPhysB/36/1161](http://stacks.iop.org/JPhysB/36/1161)

## Abstract

We measure and simulate numerically the Hanle effect and non-zero field level crossing signals in <sup>85</sup>Rb and <sup>87</sup>Rb atoms in a magnetic field at room temperature. Diode laser radiation from 4 mW cm<sup>-2</sup> to 3.3 W cm<sup>-2</sup> tuned to the D<sub>2</sub> absorption line of each isotope excites atoms into all the excited-state hyperfine levels simultaneously inside the unresolved Doppler profile. Polarization fluorescence detection is used to observe dark and bright resonances, as well as non-zero field level crossing resonances, for several excitation lines. A broad spectral line excitation model is applied to analyse the measured signals. The non-linear Zeeman effect is included in the model for both ground and excited states. Although the applied magnetic field does not exceed 80 G, several hyperfine levels of the excited state show a substantial deviation from the linear Zeeman effect.

## 1. Introduction

The Hanle effect was first presented by Hanle in *Zeitschrift für Physik* in 1924 [1]. During the following years, efforts to provide a consistent interpretation of the effect played an important role in the development of quantum theory. The essence of the Hanle effect is the creation of low frequency coherences between Zeeman magnetic sublevels of an atomic state and the destruction of these coherences by the lifting of the sublevel degeneracy by an applied magnetic field (see for example [2]).

In an atom, the fine or hyperfine levels may be split into Zeeman sublevels by an external magnetic field. A Zeeman sublevel whose energy decreases with increasing external magnetic field may cross at a particular value of magnetic field with another magnetic sublevel whose energy increases with increasing magnetic field but starts from a lower-lying (hyper)fine level (figures 1(a) and (b)). We refer to these cases as non-zero field level crossings. If atoms are excited coherently at fields corresponding to these crossing points, one can observe sub-Doppler changes of the absorption and fluorescence intensity. A theory of level crossing signals was first presented by Breit in 1936 [3], but the first experimental measurements came

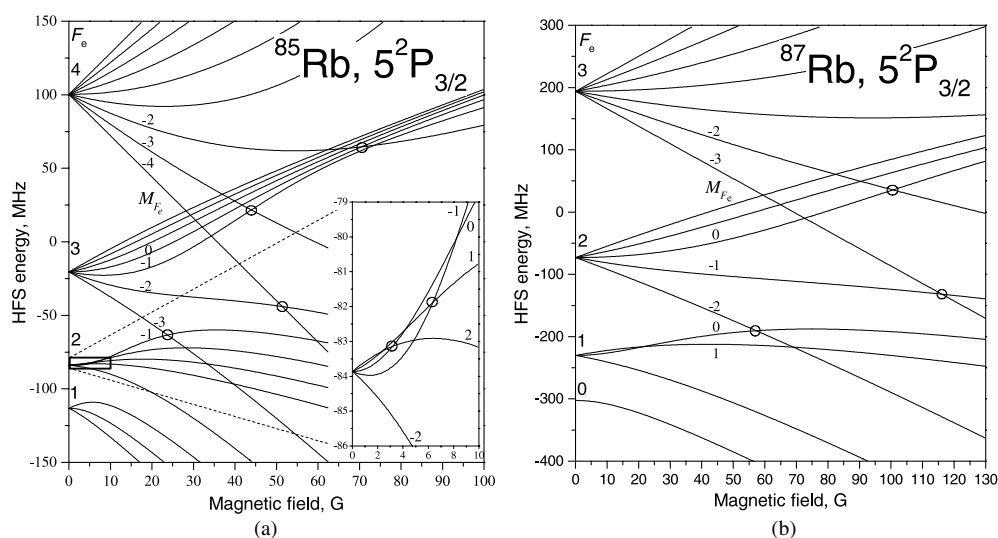


**Figure 1.** Excited-state hyperfine magnetic sublevel splitting for intermediate strength of magnetic field for  $^{85}\text{Rb}$  (a) and  $^{87}\text{Rb}$  (b) isotopes.

in 1959 with the high precision measurement of the fine structure splitting between the  $2^3\text{P}_1$  and  $2^3\text{P}_2$  states in helium [4]. A theoretical treatment of this experiment was presented later by Franken [5]. For decades, subsequent experiments used the Hanle effect to make precise measurements of the lifetimes of excited atomic states. Its extension to non-zero fields, or the level crossing technique, has allowed precise sub-Doppler measurements of fine and hyperfine constants in atoms [6].

These initial experiments using the Hanle effect only considered coherences in the excited atomic state. If the excitation is strong enough, for example if intense laser radiation is applied, coherences are also created between magnetic sublevels of the ground atomic state. An interesting effect associated with ground-state low frequency coherences is coherent population trapping, first explored by driving sodium atoms with a laser field in 1976 [7]. In coherent population trapping, destructive quantum interference between different excitation pathways traps a substantial part of the population in a coherent superposition of ground-state sublevels, i.e. dark states. Thus, coherent population trapping is associated with dark resonances, a situation in which laser light absorption and fluorescence *decreases* while the intensity of the transmitted light increases. This decrease in absorption and fluorescence can be quenched by applying an external magnetic field perpendicular to the light polarization. This field destroys the coherence between ground-state sublevels and returns the trapped atomic population into absorbing states. A review of applications of coherent population trapping and dark resonances in laser spectroscopy appears in [8].

The opposite effect, in which ground-state coherences created by a laser field *increase* laser absorption and atom fluorescence has recently been observed [9] and analysed [10, 11]. Coherences in atomic ground states have also been shown to lead to lasing without inversion [12], new methods for magnetometry [13], laser cooling [14], electromagnetically induced transparency [15], and possible coherent information storage using halted light pulses [16, 17]. These results have been matched with detailed theoretical studies, including both open systems [18] and systems with losses [19]. In this context, the ground-state Hanle effect is attracting considerable interest and intensive study [10, 11, 20, 21].

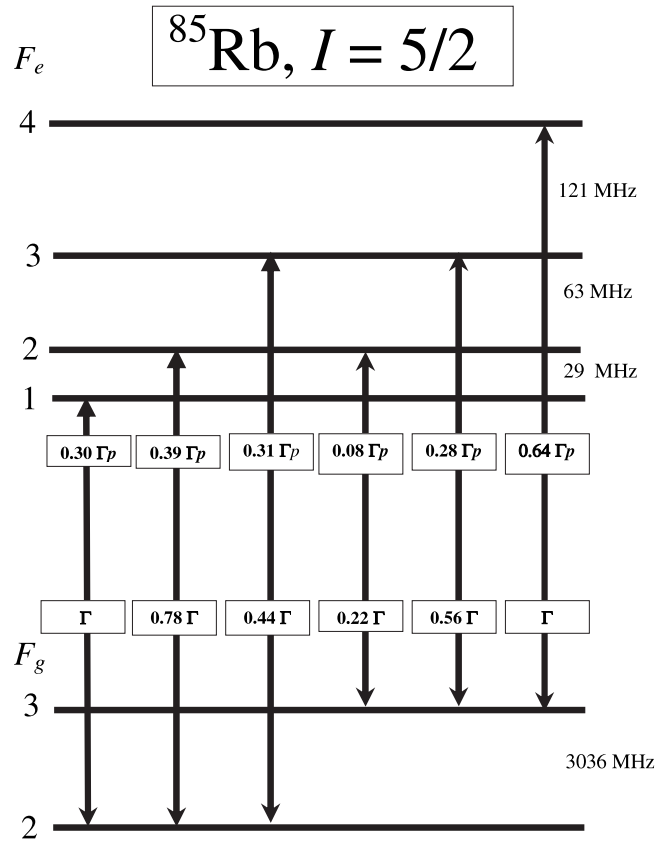


Figure 2. Hyperfine energy level splittings and relative transition probabilities for  $^{85}\text{Rb}$ .

In the present work, we study experimentally and model the polarization of the laser-induced fluorescence of Rb atoms excited by intense (up to  $3 \text{ W cm}^{-2}$ ) laser radiation. We examine two spectrally resolved ground-state hyperfine components of  $D_2$  transitions for both stable Rb isotopes. For  $^{85}\text{Rb}$ , the laser is tuned to the  $F_g = 2 \rightarrow F_e = \{1, 2, 3\}$  and  $F_g = 3 \rightarrow F_e = \{2, 3, 4\}$  absorption transitions. In  $^{85}\text{Rb}$  these components are separated by 3.036 GHz (figure 2). For  $^{87}\text{Rb}$ , the respective transitions, separated by 6.835 GHz are  $F_g = 1 \rightarrow F_e = \{0, 1, 2\}$  and  $F_g = 2 \rightarrow F_e = \{1, 2, 3\}$  (figure 3). A Rb vapour containing both isotopes at room temperature gives a Doppler line width of approximately 500 MHz. Absorption lines from each ground-state hyperfine level are separated by several gigahertz and are therefore easily resolved. The excited-state hyperfine splittings are less than 500 MHz and therefore all allowed hyperfine levels are excited simultaneously within the Doppler line width. For all transitions, the zero field (Hanle effect) as well as non-zero field level crossing signals are observed. For different transitions dark, or just the opposite—bright, resonances in the vicinity of zero magnetic field are observed and interpreted in terms of our model.

## 2. Experimental details

A 10 cm long and 2 cm diameter glass cell containing vapour of a natural abundance of Rb isotopes without buffer gas is placed in the central region of four pairs of Helmholtz coils. The coils zero the components of stray magnetic fields along three orthogonal axes and supply

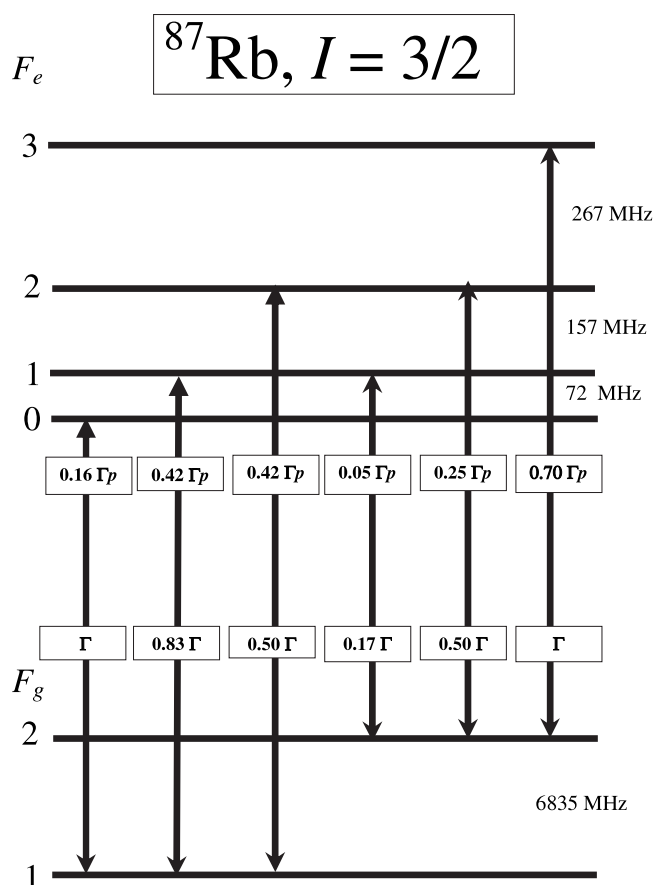


Figure 3. Hyperfine energy level splittings and relative transition probabilities for  $^{87}\text{Rb}$ .

an additional bias magnetic field. Laser radiation is directed through the cell, with both the laser polarization and the beam direction orthogonal to the applied magnetic field (figure 4). The laser radiation is produced in an extended-cavity diode laser, passing through a tapered amplifier. The strongly elliptical output is rounded using cylindrical lenses. In order to obtain high intensities, the beam is telescoped down to a 1.6 mm (measured at  $1/e^2$  intensity level) beam diameter. A retarding  $\lambda/2$  plate adjusts laser polarization. Laser beam power is 75 mW before the cell, and neutral density filters of optical density 0.08–3.0 are used for beam attenuation, resulting in laser radiation intensity in the range of 4–3300  $\text{mW cm}^{-2}$ . The diode laser line width is measured with a Fabry–Pérot etalon and found to be 5–10 MHz. By comparing sub-Doppler signals in saturated absorption spectra, we find that the tapered amplifier doubles the laser line width.

Fluorescence from a 1 cm long region of the Rb cell is observed in the direction along the magnetic field (figure 4). The distance between the fluorescence region and the detector is 15 cm, and no collection lenses are used. A polarizing beam splitter cube splits the fluorescence into two components: one parallel ( $I_{\parallel}$ ) and one perpendicular ( $I_{\perp}$ ) to the excitation laser polarization. Two photodiodes, each with an active area of  $9 \text{ mm}^2$ , collect the split fluorescence, which is amplified and subtracted. The subtracted signal is again amplified and acquired by a PC. The magnetic field is repetitively scanned ( $T = 5 \text{ s}$ ) and 32 fluorescence polarization

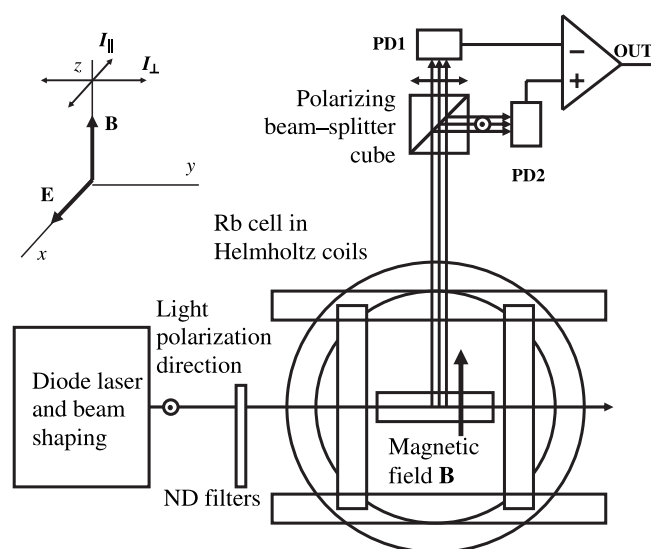


Figure 4. Scheme and geometry of the experimental setup.

signals are averaged. The laser wavelength is locked to the maximum of the Doppler profile using a separate Rb vapour cell employing a dichroic vapour lock technique [22].

A magnetic field of up to 80 G is produced in the centre of the Helmholtz coils. Each 15 cm diameter coil has 60 turns of approximately 3 mm diameter magnet wire. A 20 A, 15 V power supply is scanned from 0.3 to 18.8 A. Offset coils are installed in the main coils allowing magnetic field scans through the 0 G region. (Each offset coil has 10 turns and is run at a constant current of 3 A.) Earth and stray magnetic fields in directions orthogonal to the main field are controlled to within  $\pm 0.1$  G, as measured by a Hall magnetometer.

The measured difference signals for 4, 350, and 3300  $\text{mW cm}^{-2}$  are presented in figures 5 and 6 (curves (b)). These three signals for each transition and each isotope demonstrate the general dependence of the observed signals on the laser intensity. In addition to the Hanle signal in the vicinity of zero magnetic field, there are additional resonances at higher magnetic field values. These are attributed to non-zero field level crossings. The Hanle signal width and structure depend strongly on the particular transition. The absorption excitation signals from the lower hyperfine levels are much broader than signals registered from the upper hyperfine component. For the absorption curve from the lower hyperfine level in  $^{85}\text{Rb}$ , a dip very close to zero magnetic field can be seen. Such a dip is not present in the  $^{87}\text{Rb}$  spectra. In absorption from the upper ground-state hyperfine components, the Hanle signals are substantially narrower. In some cases (e.g.  $^{87}\text{Rb}$ , figure 6 case 4), a clearly pronounced high contrast peak in the vicinity of zero magnetic field is observed. Non-zero field level crossing signals in all cases have more or less the same width, but their relative size in comparison to the zero-field Hanle signal decreases with increasing laser light intensity.

### 3. Model

The most detailed description of an interaction of coherent laser radiation with gaseous atoms can be achieved with the help of the optical Bloch equations [8]. However, in our experiment the excitation laser line width after tapered amplifier ( $\propto 10\text{--}20$  MHz) is larger than the natural

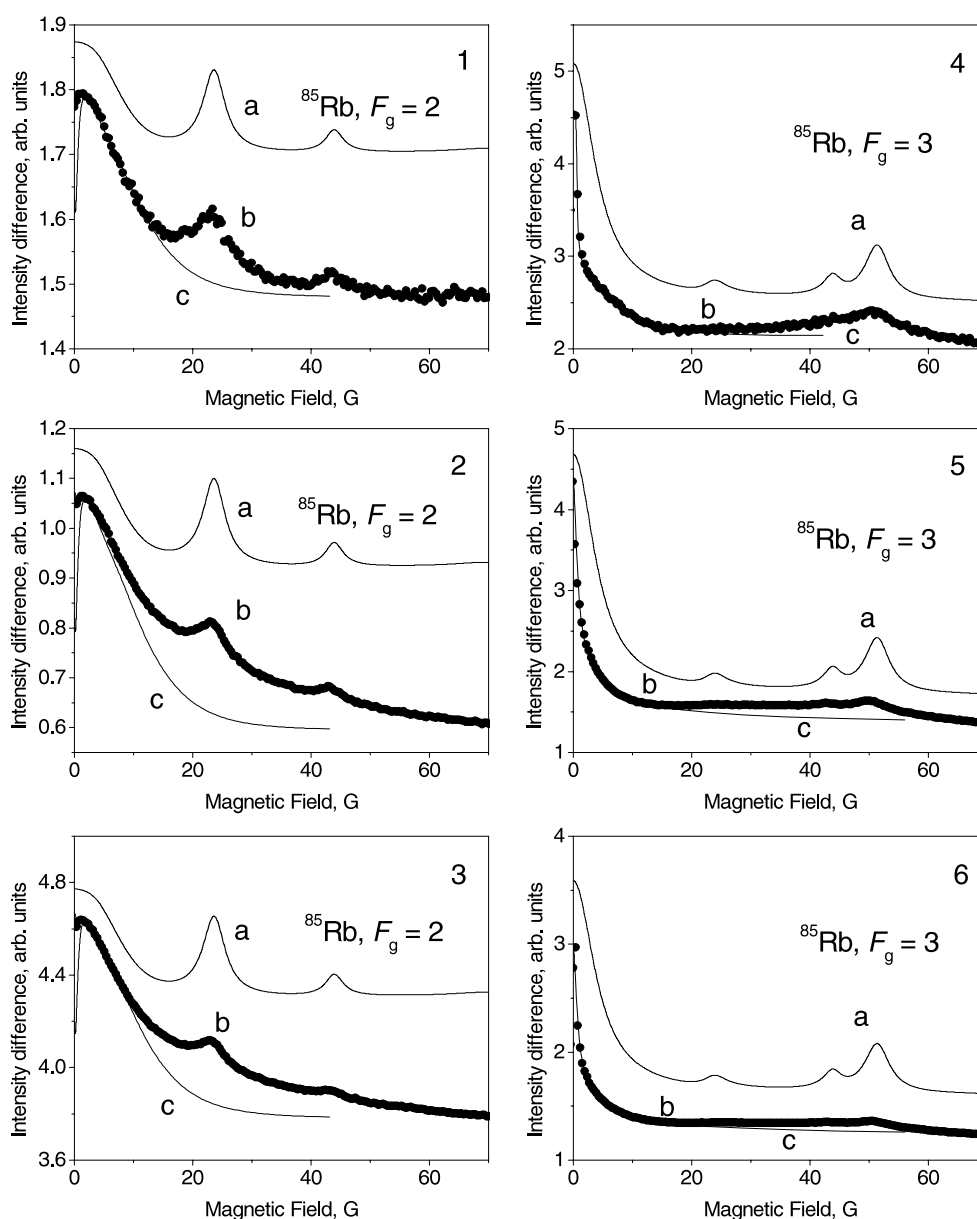


**Figure 5.** Measured and simulated zero and non-zero field level crossing signals for  $^{85}\text{Rb}$ . Curves (b) are experimentally detected signals. The intensity is  $4 \text{ mW cm}^{-2}$  in curves 1(b) and 4(b),  $350 \text{ mW cm}^{-2}$  in 2(b) and 5(b), and  $3300 \text{ mW cm}^{-2}$  in 3(b) and 6(b). Curves (a) and (c) are the result of numerical calculations corresponding to the strong and weak magnetic field models respectively. For curves (c),  $\Gamma_p$  is  $38 \times 10^6 \text{ s}^{-1}$  for curves 1–4(c) and  $760 \times 10^6 \text{ s}^{-1}$  for 5(c) and 6(c). The curves are shifted vertically for clarity.

line width of the absorption transition (6 MHz) which means that in this particular case we have a broad-band laser with relatively poor coherence properties [23–25]. Thus we initially use a broad-line excitation model to treat the problem [26, 27]. Although this approach was initially

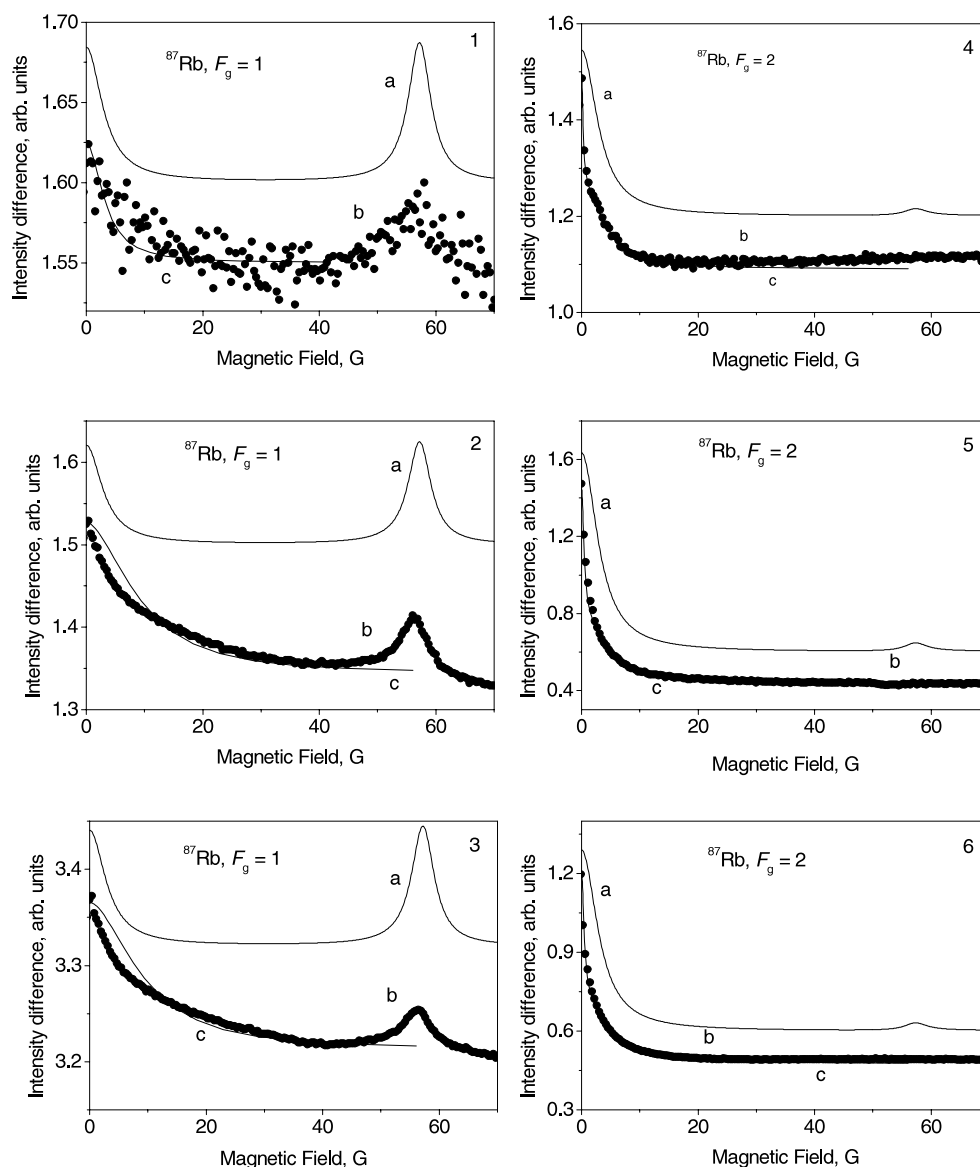


**Figure 6.** Measured and simulated zero and non-zero field level crossing signals for  $^{87}\text{Rb}$ . Curves (b) are experimentally detected signals. The intensity is  $4 \text{ mW cm}^{-2}$  in curves 1(b) and 4(b),  $350 \text{ mW cm}^{-2}$  in 2(b) and 5(b), and  $3300 \text{ mW cm}^{-2}$  in 3(b) and 6(b). Curves (a) and (c) are the result of numerical calculations corresponding to the strong and weak magnetic field models respectively. For curves (c),  $\Gamma_p$  is  $38 \times 10^6 \text{ s}^{-1}$  for curves 1(c) and 4(c),  $3800 \times 10^6 \text{ s}^{-1}$  for curves 2(c) and 3(c), and  $100 \times 10^6 \text{ s}^{-1}$  for 5(c) and 6(c). The curves are shifted vertically for clarity.

developed for a weak radiation case [26] and does not account for optical coherences created by the laser radiation in an atomic ensemble, it is more simple than an approach based on optical Bloch equations and in many cases it obtains a satisfactory description of multi-mode laser light interaction with gases. Recently, it was applied successfully to Rb and Cs atoms [11, 21] excited with spectrally broad radiation from diode lasers. In the case of molecules, it is used

extensively [27, 33–35], even in the case of a rather intense laser field when lasers operate in a multimode regime.

The equations presented below describe atom interactions with laser radiation in the broad spectral line approximation. The equations of motion for the density matrix in the broad-line limit read

$$\begin{aligned} \dot{f}_{M_e M'_e} = & \Gamma_p \sum_{M_g M'_g} \langle M_e | \mathbf{E}^* \mathbf{d} | M_g \rangle \langle M'_e | \mathbf{E}^* \mathbf{d} | M'_g \rangle^* \varphi_{M_g M'_g} \\ & - \frac{\Gamma_p}{2} \sum_{M'_e M_g} \langle M_e | \mathbf{E}^* \mathbf{d} | M_g \rangle \langle M'_e | \mathbf{E}^* \mathbf{d} | M_g \rangle^* f_{M'_e M'_e} \\ & - \frac{\Gamma_p}{2} \sum_{M'_e M_g} \langle M'_e | \mathbf{E}^* \mathbf{d} | M_g \rangle \langle M_e | \mathbf{E}^* \mathbf{d} | M_g \rangle^* f_{M_e M'_e} \\ & - \Gamma f_{M_e M'_e} - i\omega_{M_e M'_e} f_{M_e M'_e} \end{aligned} \quad (1)$$

$$\begin{aligned} \dot{\varphi}_{M_g M'_g} = & -\frac{\Gamma_p}{2} \sum_{M'_g M_e} \langle M_g | \mathbf{E}^* \mathbf{d} | M_e \rangle \langle M'_g | \mathbf{E}^* \mathbf{d} | M_e \rangle^* \varphi_{M'_g M'_g} \\ & - \frac{\Gamma_p}{2} \sum_{M'_g M_e} \langle M'_g | \mathbf{E}^* \mathbf{d} | M_e \rangle \langle M_g | \mathbf{E}^* \mathbf{d} | M_e \rangle^* \varphi_{M_g M'_g} \\ & + \Gamma_p \sum_{M_e M'_e} \langle M_g | \mathbf{E}^* \mathbf{d} | M_e \rangle \langle M'_g | \mathbf{E}^* \mathbf{d} | M'_e \rangle^* f_{M_e M'_e} \\ & - \gamma \varphi_{M_g M'_g} - i\omega_{M_g M'_g} \varphi_{M_g M'_g} + \sum_{M_e M'_e} \Gamma_{M_g M'_g}^{M_e M'_e} f_{M_e M'_e} + \lambda \delta_{M_g M'_g} \end{aligned} \quad (2)$$

where  $f_{M_e M'_e}$  and  $\varphi_{M_g M'_g}$  are the density matrices of the excited- and ground-state levels respectively. The first term on the right-hand side of equation (1) accounts for the absorption of light at rate  $\Gamma_p$ . For the transition matrix elements of the form  $\langle M_e | \mathbf{E}^* \mathbf{d} | M_g \rangle$ ,  $\mathbf{E}$  is the light polarization vector and  $\mathbf{d}$  is the dipole operator. The second and third terms describe stimulated emission. The fourth term characterizes the relaxation of the density matrix  $f_{M_e M'_e}$  with a rate  $\Gamma$ . Finally, the fifth term describes the Zeeman splitting of the magnetic sublevels  $M_e$  and  $M'_e$  by a value of  $\omega_{M_e M'_e} = (E_{M_e} - E_{M'_e})/\hbar$ .

The first and second terms on the right-hand side of equation (2) describe light absorption, the third term the stimulated light emission, and the fourth term the relaxation processes in the ground state of rate  $\gamma$ . The fifth term characterizes the Zeeman interaction, the sixth term represents the repopulation of the initial level by spontaneous transitions at a rate  $\Gamma_{M_g M'_g}^{M_e M'_e}$ , and the seventh term the relaxation of the density matrix of the ground-state atoms interacting with the gas in the cell at a rate  $\lambda$ . Under conditions of stationary excitation, the system of equations (1) and (2) becomes a system of linear equations for the ground- and excited-state density matrix elements.

The matrix elements of the type  $\langle M_e | \mathbf{E}^* \mathbf{d} | M_g \rangle$  can be calculated using standard angular momentum algebra [27–29]. In general, the ground-state relaxation rate  $\gamma$  includes atom–atom collisions, collisions with the walls, and fly-through relaxation (relaxation due to atoms exiting the beam interaction region). In our particular case, fly-through relaxation was the main relaxation mechanism. All atoms exiting the probe region with a coherence in the ground state are replaced by atoms that have not interacted with radiation. The fly-through relaxation rate for Rb at room temperature and a laser beam diameter of several millimetres is approximately  $0.2 \times 10^6 \text{ s}^{-1}$ . Rb atom concentration at room temperature is approximately  $7 \times 10^9 \text{ atoms cm}^{-3}$  [30] which makes collisional relaxation and radiation reabsorption

negligible. The fly-through relaxation rate is small compared to the rate of spontaneous emission. Nevertheless, it must be included in the excited-state relaxation rate  $\Gamma = \Gamma_{F_e F_g} + \gamma$  to conserve the total number of atoms cycling between the ground and excited states. The relative probabilities of optical transitions between hyperfine sublevels are given by [31]:

$$W_{F_g \rightarrow F_e} = (2F_e + 1)(2F_g + 1)(2J_e + 1)(2J_g + 1) \begin{Bmatrix} J_g & F_g & I \\ F_e & J_e & 1 \end{Bmatrix}^2 \begin{Bmatrix} L_g & J_g & S \\ J_e & L_e & 1 \end{Bmatrix}^2. \quad (3)$$

In a sufficiently strong external magnetic field, the ground- and excited-state levels  $\chi_g$  and  $\chi_e$  are not characterized by total angular momentum quantum numbers  $F_g$  and  $F_e$ , but are instead mixtures of these states,

$$|\chi_e, M_e\rangle = \sum_{F_e=J_e-I}^{F_e=J_e+I} C_{\chi_e F_e}^{(e)} |F_e, M_e\rangle, \quad |\chi_g, M_g\rangle = \sum_{F_g=J_g-I}^{F_g=J_g+I} C_{\chi_g F_g}^{(g)} |F_g, M_g\rangle. \quad (4)$$

Here, the expansion coefficients  $C_{\chi_e F_e}^{(e)}$ ,  $C_{\chi_g F_g}^{(g)}$  represent the mixing of unperturbed hyperfine states by the magnetic field. While  $F$  ceases to be a good quantum number, the magnetic quantum number  $M$  is still valid. The expansion coefficients  $C_{\chi_e F_e}^{(e)}$ ,  $C_{\chi_g F_g}^{(g)}$ , along with the magnetic sublevel energy splitting  $\Delta\omega_{M_i M_i'}(B) = [E_{M_i}(B) - E_{M_i'}(B)]/\hbar$  can be obtained by diagonalization of the Hamiltonian matrix (see for example [32]). For the  $5^2P_{3/2}$  state of  $^{85}\text{Rb}$  and  $^{87}\text{Rb}$  these magnetic sublevel splittings are presented in figures 1(a) and (b).

The contribution of the fluorescence signal from each allowed hyperfine transition is calculated according to [27]:

$$I = I_o \sum_{M_e M_e' M_g} \langle M_e | (\mathbf{E}')^* \mathbf{d} | M_g \rangle \langle M_e' | (\mathbf{E}')^* \mathbf{d} | M_g \rangle^* f_{M_e M_e'} \quad (5)$$

where  $\mathbf{E}'$  is the polarization of the observed light, and  $I_o$  is an experiment-dependent coefficient. Allowing for mixing of the hyperfine states and summing over all transitions we find the experimentally observed polarization-dependent fluorescence to be [32],

$$I(\mathbf{E}_f) = I_o \sum_{M_e M_e' M_g} \sum_{\chi_e \chi_e' \chi_g} \langle \chi_e M_e | \hat{\mathbf{E}}_f^* \cdot \hat{\mathbf{d}} | \chi_g M_g \rangle \langle \chi_e' M_e' | \hat{\mathbf{E}}_f^* \cdot \hat{\mathbf{d}} | \chi_g M_g \rangle^* \chi_e \chi_e' f_{M_e M_e'}. \quad (6)$$

Our analysis is not sensitive to  $I_o$  since only normalized spectra are considered. Finally, we assume that transition probabilities are not substantially affected by the level mixing in a magnetic field.

The numerical simulation of equations (1) and (2) for the model described above is very cumbersome for arbitrary magnetic fields. Next, we break the model into two parts: a weak magnetic field model to analyse the Hanle signals as the magnetic field approaches zero and a strong magnetic field model to find the exact positions of expected non-zero field level crossing resonances.

## 4. Zeeman effect

### 4.1. Weak magnetic field model

In a weak magnetic field, which will be used to describe the Hanle effect at fields  $\leq 10$  G, the magnetic level splitting is small in comparison with the hyperfine splitting (figure 1). We assume that the hyperfine level mixing described by equation (4) is negligible and  $F$  is still a good quantum number (i.e.  $C_{\chi F} = \delta_{\chi F}$ ). However, we still incorporate the non-linear Zeeman effect for the calculation of *energies*. For some magnetic sublevels, for example  $F_e = 2$  in  $^{85}\text{Rb}$ , this non-linearity can be considerable even for magnetic field strengths of  $\leq 10$  G (see

figure 1(a)). We also assume, because the hyperfine splittings of the excited- and ground-state levels (see figures 2 and 3) are substantially larger than the laser line width and the homogeneous line width of the absorbing transition, that each hyperfine transition is excited independently. In other words, it is assumed that different  $F_g \leftrightarrow F_e$  transitions are not coupled by the laser field. For a given laser frequency, each  $F_g \leftrightarrow F_e$  transition is associated with a different velocity class.

With these assumptions, the excited-state density matrix elements are obtained as the steady-state solution to equations (1) and (2). After obtaining the excited-state density matrix, the polarization-dependent fluorescence intensity is calculated according to equation (6), and the simulated  $I_{\parallel} - I_{\perp}$  signals are determined and shown in figures 5 and 6 (curves (c)). To obtain these curves,  $\Gamma_p$  is adjusted for best fit to the data (see section 4). The Hanle resonances we simulate are similar to the ground-state Hanle signals previously studied in molecules [27, 33–35]. In molecules for open optical pumping cycles, different dark and bright resonances were observed in an external magnetic field and interpreted quantum mechanically. These results were also accurately modelled classically, since the angular momentum quantum number easily reached values of the order of 100.

#### 4.2. Strong magnetic field model

As the magnetic field strength increases, we must include the mixing of hyperfine states given in equation (4). Additionally, for the coherently excited non-zero field level crossings, we cannot assume that different  $\chi_e \leftrightarrow \chi_g$  transitions are excited independently. For these field values we must take into account simultaneous coherent excitation of magnetic sublevels initially belonging to different hyperfine levels of the excited-state manifold using equation (7). To simplify the task for the case of strong magnetic field, we assume that the laser light does not create coherences in the ground-state  $\chi_g$ . Although this assumption is only approximately true for the magnetic field strengths under consideration, it allows us to find the exact positions and approximate relative amplitudes and line widths for expected non-zero field level crossing resonances. Specifically, the assumption of a non-coherent ground-state population allows us to write the excited-state density matrix as

$$\rho_{M_e M'_e}^{\chi_e \chi'_e} = \frac{\Gamma_p}{\Gamma + i\chi_e \chi'_e \Delta\omega_{M_e M'_e}} \sum_{\chi_g M_g} \langle \chi_e M_e | \hat{\mathbf{E}}_{exc}^* \cdot \hat{\mathbf{d}} | \chi_g M_g \rangle \langle \chi'_e M'_e | \hat{\mathbf{E}}_{exc} \cdot \hat{\mathbf{d}} | \chi_g M_g \rangle^*. \quad (7)$$

Here  $\chi_e \chi'_e \Delta\omega_{M_e M'_e} = (\chi_e E_{M_e} - \chi'_e E_{M'_e})/\hbar$  is the energy splitting of magnetic sublevels  $M_e$  and  $M'_e$  belonging to the excited-state levels  $\chi_e$  and  $\chi'_e$ . For details of this approach see [32]. The simulated  $I_{\parallel} - I_{\perp}$  fluorescence is obtained by substituting equation (7) into (6), and is shown by curves (a) in figures 5 and 6. The locations of these resonances are determined by the excited-state magnetic sublevel crossing points (circles in figures 1(a) and (b)). The ground-state magnetic sublevels belonging to different hyperfine levels do not undergo crossings.

### 5. Results and analysis

The experimental results are given by curves (b) in figures 5 and 6. For both isotopes, signals from the lower ground-state hyperfine level are broader than the signals from the upper ground-state hyperfine level. For atoms in the lower hyperfine level of the ground state, only the transition to the  $F_e = F_g - 1$  state is a closed or cycling transition. For the other two transitions, atoms are quickly optically pumped into the other hyperfine level and no longer participate in the absorption–fluorescence process. Since the  $F_e = F_g - 1$  transition occurs with significantly less loss, we expect that the fluorescence from it will dominate the observed

averaged fluorescence intensity. Dark resonances are expected to occur in this transition [8], thus the fluorescence intensity should increase when the magnetic field destroys the dark state. We clearly see this behaviour in the case of  $^{85}\text{Rb}$   $F_g = 2$  (figure 5), though it is less pronounced in the experiment than in the simulated signal. We believe the experimental resonance is degraded by averaging over many magnetic field scans. (The reproduction accuracy of the magnetic field is  $\pm 0.5$  G.) For  $^{87}\text{Rb}$   $F_g = 1$  no dark resonance is observed (figure 6) because the closed transition excites to  $F_e = F_g - 1 = 0$ . The  $F_e = 0$  excited level is spherically symmetric and radiates both polarizations isotropically, and therefore does not contribute to the  $I_{\parallel} - I_{\perp}$  signal.

For transitions that start from the upper ground-state hyperfine level, the closed or cycling transition excites to the  $F_e = F_g + 1$  state. In this case the closed transition exhibits a bright resonance [10, 11, 21]. In figures 5 and 6, case 4, the signal shows the bright resonance at relatively low laser intensity when signals are not substantially power broadened by laser radiation. In the experiment (curve (b)) a narrow feature arises on top of the broad Hanle signal. In cases 5 and 6, the bright resonance broadens, but the signals in the vicinity of zero magnetic field still exhibit structure narrower than the ordinary Hanle signal represented by curve (a).

To analyse non-zero field level crossing signals, we compare experimental signals with simulated excited-state level crossing signals using the strong-field model, represented by curves (a) in figures 5 and 6. The position and width of the non-zero field level crossing signals are represented very well in all cases. The amplitudes of these features are in qualitative agreement with experiment at low laser intensity. However, as the laser intensity increases, the resonances disappear from the experimental data but remain constant in the model. The model fails here because it neglects ground-state coherences. In the absence of these coherences, the hyperfine population distribution of the ground state is not affected by the intensity of the laser radiation. However, at the non-zero magnetic fields where the crossings take place, the hyperfine level mixing destroys the pure cycling (closed) transition. Therefore, other hyperfine states are admixed to the excited-state level initially belonging to the cycling transition, and both ground-state hyperfine levels access all excited states. Increasing laser intensity enhances this effect because it makes optical pumping more effective.

We now discuss the absorption rate  $\Gamma_p$  values used to fit experimental signals with simulated curves. The laser intensity in the experiment varied from  $4 \text{ mW cm}^{-2}$  up to  $3300 \text{ mW cm}^{-2}$ . For a laser intensity of  $4 \text{ mW cm}^{-2}$ ,  $\Gamma_p = 38 \times 10^6 \text{ s}^{-1}$  provides the best fit to the experimental data and corresponds well to the estimate made from the following simple model: if we assume that the cycling transition rate  $\Gamma_p$  coincides with the spontaneous transition rate  $\Gamma$ , the following relation between the respective Einstein coefficients exists:

$$\Gamma_p = B_{eg}u = A_{eg} = \Gamma, \quad (8)$$

where  $u$  is the spectral density of the radiation ( $\text{erg cm}^3 \text{ Hz}^{-1}$ ). Using the relationship between the spectral intensity and density,  $dI/d\nu = uc$  ( $\text{W (Hz cm}^2)^{-1}$ ), and the relation between Einstein coefficients we obtain,

$$dI/d\nu = \frac{8\pi h\nu^3}{c^2}. \quad (9)$$

Given that the natural (homogeneous) line width of the absorbing line at the half-maximum is  $\Delta\nu = \Gamma/2\pi$ , we calculate the saturation intensity (the laser intensity that drives stimulated emission at the same rate as spontaneous emission),

$$I_{sat} = \frac{4h\nu_{eg}^3}{c^2}\Gamma = \frac{4hc}{\lambda_{eg}^3}\Gamma. \quad (10)$$

Assuming the spontaneous emission rate for Rb is  $\Gamma = 38 \times 10^6 \text{ s}^{-1}$ ,  $I_{sat}$  is approximately  $3 \text{ mW cm}^{-2}$ . If the laser line width is much broader than the homogeneous absorption line width, then the laser intensity needed for saturation is  $dI/d\nu = 8\pi h\nu^3/c^2$  times the laser line width  $\Delta f$ . Numerical estimates show that in the intermediate case relevant here, the laser line width being slightly broader than the natural line width,  $I_{sat}$  is approximately  $4 \text{ mW cm}^{-2}$ . Thus, the saturation condition  $\Gamma_p/\Gamma \propto 1$  holds, even for the lowest laser intensity considered in the experiment.

In fitting the model to the experimental data as shown in figures 5 and 6, we find that the effective  $\Gamma_p$  increases more slowly than linearly with increasing peak laser intensity. This effect may be understood by considering the Gaussian wings of both the spatial distribution of the laser and the velocity distribution of the ensemble of atoms.

## 6. Summary

We have experimentally as well as theoretically studied bright and dark resonances in the Hanle effect as well as non-zero field level crossing resonances in both Rb isotopes for a broad range of laser intensities. The observed signals in the polarization of the laser-induced fluorescence have been modelled using a broad excitation line approach, and account has been taken of the non-linear Zeeman effect, optical pumping, ground-state low frequency coherences at low magnetic field, and magnetic field mixing of hyperfine states at high magnetic field. A model using the optical Bloch equations to take into account optical coherences may be developed in the future.

## Acknowledgments

We acknowledge support from the National Science Foundation and the United States Office of Naval Research. Travel support for MA was provided by the University of Oklahoma. KB would like to thank Girts Folkmanis for valuable assistance in the development of the computer code for signal simulation.

## References

- [1] Hanle W 1924 *Z. Phys.* **30** 93
- [2] Moruzzi G and Strumia F (ed) 1991 *The Hanle Effect and Level-Crossing Spectroscopy* (New York: Plenum) (Engl. transl.)
- [3] Breit G 1936 *Rev. Mod. Phys.* **5** 91
- [4] Colgrove F D, Franken P A, Lewis R R and Sands R H 1959 *Phys. Rev. Lett.* **3** 420
- [5] Franken P A 1961 *Phys. Rev.* **121** 508
- [6] Arimondo E, Inguscio M and Violino P 1977 *Rev. Mod. Phys.* **49** 31
- [7] Alzetta G, Gozzini A, Moi L and Orriols G 1976 *Nuovo Cimento B* **36** 5
- [8] Arimondo E 1996 *Prog. Opt.* **35** 257
- [9] Dancheva Y, Alzetta G, Cartaleva S, Taslakov M and Andreeva Ch 2000 *Opt. Commun.* **178** 103
- [10] Renzoni F, Zimmermann C, Verkerk P and Arimondo E 2001 *J. Opt. B: Quantum Semiclass. Opt.* **3** S7
- [11] Alnis J and Auzinsh M 2001 *J. Phys. B: At. Mol. Opt. Phys.* **34** 3889
- [12] Scully M, Zhu S-Y and Gavrielides A 1989 *Phys. Rev. Lett.* **62** 2813
- [13] Scully M and Fleischhauer M 1992 *Phys. Rev. Lett.* **69** 1360
- [14] Aspect A, Arimondo E, Kaiser R, Vansteenkiste N and Cohen-Tannoudji C 1988 *Phys. Rev. Lett.* **61** 826
- [15] Harris S 1997 *Phys. Today* **50** 36
- [16] Philips D F, Fleischhauer A, Mair A, Walsworth R L and Lukin M D 2001 *Phys. Rev. Lett.* **86** 783
- [17] Liu C, Dutton Z, Behroozi C H and Hau L V 2001 *Nature* **409** 490
- [18] Renzoni F, Lindner A and Arimondo E 1999 *Phys. Rev. A* **60** 450
- [19] Renzoni F, Maichen W, Windholz L and Arimondo E 1997 *Phys. Rev. A* **55** 3710

- [20] Renzoni F, Cartaleva S, Alzetta G and Arimondo E 2001 *Phys. Rev. A* **63** 065401
- [21] Papojan A V, Auzinsh M and Bergmann K 2002 *Eur. Phys. J. D* **21** 63
- [22] Corwin K L, Lu Z-T, Hand C F, Epstein R J and Wieman C E 1998 *Appl. Opt.* **37** 3295
- [23] Shore B W 1995 *The Theory of Coherent Atomic Excitation* (New York: Wiley)
- [24] Vitanov N V, Fleischhauer M, Shore B W and Bergmann K 2001 *Adv. At. Mol. Opt. Phys.* **46** 55
- [25] Vitanov N V, Halfmann T, Shore B W and Bergmann K 2001 *Ann. Rev. Phys. Chem.* **52** 763
- [26] Cohen-Tannoudji C 1962 *Ann. Phys., Paris* **7** 423  
Cohen-Tannoudji C 1962 *Ann. Phys., Paris* **7** 469
- [27] Auzinsh M and Ferber R 1995 *Optical Polarization of Molecules* (Cambridge: Cambridge University Press)
- [28] Varshalovich D A, Moskalev A N and Khersonskii V K 1988 *Quantum Theory of Angular Momentum* (Singapore: World Scientific)
- [29] Zare R N 1988 *Angular Momentum, Understanding Spatial Aspects in Chemistry and Physics* (New York: Wiley)
- [30] Nesmeyanov A N 1963 *Vapor Pressure of the Chemical Elements* ed R Gary (Amsterdam: Elsevier)
- [31] Sobelman I I 1979 *Atomic Spectra and Radiative Transitions* (Berlin: Springer)
- [32] Alnis J and Auzinsh M 2001 *Phys. Rev. A* **63** 023407
- [33] Auzinsh M P and Ferber R S 1991 *Phys. Rev. A* **43** 2374
- [34] Auzinsh M P and Ferber R S 1990 *Sov. Phys.-Usp.* **33** 833
- [35] Auzinsh M P and Ferber R S 1983 *Opt. Spectrosc. (USSR)* **55** 674